Effect of the plasmonic dispersion relation on the transmission properties of subwavelength cylindrical holes

Hocheol Shin, Peter B. Catrysse, and Shanhui Fan
Department of Electrical Engineering, Stanford University, Stanford, California 94305, USA
(Received 21 March 2005; published 16 August 2005)

We analyze subwavelength cylindrical holes in an optically thick metallic film with the metal described by a plasmonic model. We find that the dispersion diagram exhibits three distinct features that have a profound impact on the transmission of incident light through cylindrical holes. First, such holes always support propagating modes near the surface plasmon frequency, regardless of how small the holes are. Second, the fundamental plasmonic mode (HE_{11}) is located completely below the surface plasmon frequency and gives rise to a passband in the transmission spectrum. Third, when the radius of the holes is small, there exists a stop band, just above the surface plasmon frequency, where a normally incident plane wave does not transmit. Based on the dispersion analysis, we design both a single hole and a hole array in which propagating modes play a dominant role in the transport properties of incident light. These structures exhibit a different region of operation that has not been probed yet experimentally, while featuring a high packing density and diffractionless behavior.

DOI: 10.1103/PhysRevB.72.085436 PACS number(s): 78.20.Bh, 42.25.Fx, 42.25.Bs, 41.20.Jb

I. INTRODUCTION

The optical properties of nanoapertures in an optically thick metallic film have been intensely researched in the past several years due to their fundamental importance in near-field optics, and their practical significance to photonic devices and applications, including filters, near-field probes, and optical data storage.[1] It is well known that the transmission characteristics are strongly influenced by the presence or absence of propagating modes inside the apertures.[2,3] In metallic nanoslits, enhanced transmission has been attributed to propagating transverse magnetic (TM) modes inside the slits.[2,4–8] For cylindrical holes, such as those featured in Ebbesen *et al.*'s original experiments,[9] the spectral features have been shown to be largely independent of the material used for the vertical walls of the hole.[10,11] Therefore, the prevailing wisdom is that cylindrical holes do not support propagating modes when the hole diameter is smaller than $\approx\lambda/2n_0$, where λ is the wavelength of incident light and n_0 is the refractive index of the material inside the hole.[12,13] Instead, enhanced transmission is commonly associated with an excitation of surface wave resonances on the front and back surfaces of the metallic film, and an evanescent tunneling process through the holes between these resonances.[9,11,13–16]

In this paper, we investigate the effect of the dispersion relation on the transmission properties of subwavelength cylindrical holes in an optically thick metallic film. We describe the optical properties of the metal using a Drude free-electron model:

$$\varepsilon_2(\omega) = 1 - \frac{\omega_p^2}{\omega(\omega - i\omega_\tau)}, \tag{1}$$

where ω_p is the plasma frequency and ω_τ is the collision frequency. In this model, the dielectric function takes into account the contribution of free electrons only and displays plasma-like dispersion. Hence, we refer to it as a *plasmonic model*. Despite its apparent simplicity, the plasmonic model has been the source of valuable insights into the behavior of real metals. For aluminum and most alkali metals, its regime of validity extends deep into the visible wavelength regime.[17] In describing the optical behavior of noble metals (e.g., silver, gold, copper), it has proven to be accurate in the near- and far-infrared wavelength regime,[18,19] while being a reasonable approximation in the visible wavelength range above 500 nm. By allowing for additional Lorentzian resonance terms, its use can be easily extended to the entire visible wavelength range, i.e., below 500 nm, where interband transitions often contribute to the dielectric function.[20,21] While a model extension of this type might be more realistic and result in applicability to a larger group of metals in a wider wavelength range, its study is beyond the scope of this paper. Here, we study the optical behavior of subwavelength cylindrical holes in an optically thick metallic film when the metal is described using the plasmonic model. We compare and contrast it to the optical behavior predicted by the often-used perfect electric conductor (PEC) model.[2,4,22,23] For a cylindrical waveguide, it has been shown that the dispersion relation is qualitatively different for a plasmonic model as opposed to a PEC model.[21] To the best of our knowledge, however, the importance of a plasmonic dispersion relation for the transport of incident light through subwavelength cylindrical holes has never been recognized.

The main findings of our work are summarized as follows. We find that the plasmonic dispersion diagram exhibits three distinct features that have a profound impact on the transmission of incident light through cylindrical holes. First, such holes always support propagating modes near the surface plasmon frequency, *regardless of how small the holes are*. Even when material losses are included as part of the plasmonic model, the modes still propagate over several micrometers when the radius of the holes is much smaller than $\lambda/2n_0$. Second, the fundamental (lowest-frequency) mode has a HE_{11} signature, which enables it to couple to a nor-

 ©2005 The American Physical Society

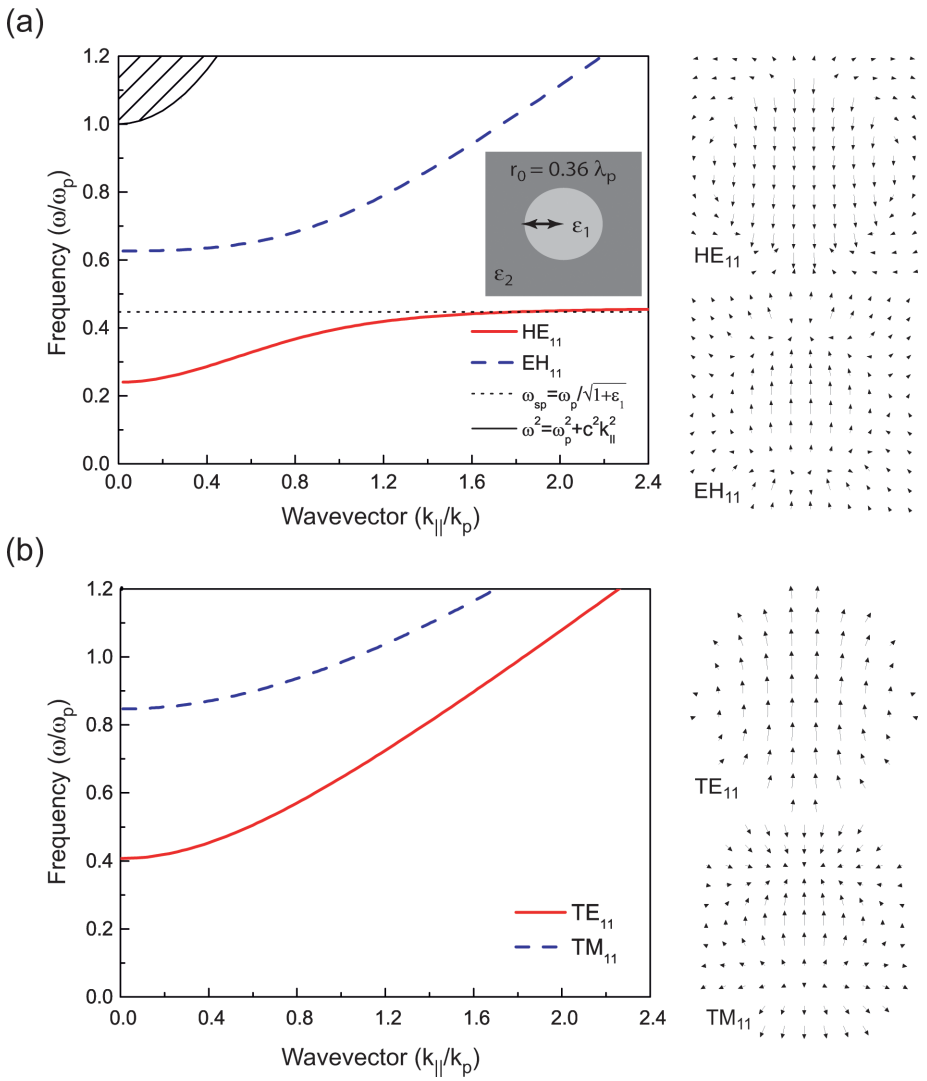

FIG. 1. (Color) Dispersion diagram for a cylindrical hole with radius $0.36\lambda_p$, where λ_p is the plasma wavelength. (a) Dispersion relations of the two lowest-order waveguide modes with angular momentum $m=1$ for a plasmonic model. The solid red line corresponds to the dispersion of the HE_{11} mode, while the dashed blue line shows the dispersion of the EH_{11} mode. Insets show the vector plots for the electric fields of the HE_{11} and the EH_{11} mode, respectively. (b) Dispersion relations of the two lowest-order waveguide modes with angular momentum $m=1$ assuming a perfect electric conductor (PEC) model. The featured modes are TE_{11} (solid red line) and TM_{11} (dashed blue line). Insets show the vector plots for the electric fields of the TE_{11} and the TM_{11} mode, respectively.

mally incident plane wave. The HE_{11} mode is located completely below the surface plasmon frequency of the metal-dielectric interface. Thus, a cylindrical hole in a plasmonic metal always exhibits a passband below the surface plasmon frequency. Third, when the radius of the hole is small, there exists a stop band for a normally incident plane wave, where the light does not transmit. The location of this band is just above the surface plasmon frequency. Hence, a single hole or a hole array may behave as a bandpass filter and allow longer wavelengths to pass through while rejecting shorter ones. All of these features are fundamentally different from the behavior of the PEC model. Furthermore, they cannot be explained by a PEC model, even when such a model uses an effective hole radius, which is derived from a skin depth calculation.

Based on the dispersion analysis, we use three-dimensional (3D) finite-difference time-domain (FDTD) simulations to investigate the transmission of both single holes and hole array structures in which propagating modes play a dominant role in the transport properties of incident light. These structures feature a high packing density and diffractionless behavior, and they exhibit a different region of operation that has not been probed yet experimentally.

II. ANALYSIS OF PROPAGATING MODES

To calculate the propagating modes inside a cylindrical hole, we consider a z-invariant waveguide with a cylindrical cross section of radius r_0 in the transverse xy plane [Fig. 1(a) inset]. For the dielectric inside the hole, we use a real, frequency-independent dielectric function ε_1. For the surrounding metal, we define a frequency-dependent dielectric function ε_2. The mode (m,n) of the waveguide is found by solving Maxwell's equations in cylindrical coordinates for electric and magnetic fields of the form $\psi(r,\phi,z,t)$

$=\psi_n(r)\exp(jm\phi)\exp[j(\omega t-k_\parallel z)]$, where m is an integer denoting angular momentum, n is related to the number of nodes in the radial direction, while ω and $k_\parallel$ are the frequency and the wave vector of a mode in the hole. By matching boundary conditions, a transcendental equation is obtained as the dispersion relation[24]

$$\left[\frac{\varepsilon_1}{k_{T,1}}\frac{J_m'}{J_m}-\frac{\varepsilon_2}{k_{T,2}}\frac{H_m^{(1)'}}{H_m^{(1)}}\right]\left[\frac{1}{k_{T,1}}\frac{J_m'}{J_m}-\frac{1}{k_{T,2}}\frac{H_m^{(1)'}}{H_m^{(1)}}\right]=m^2\frac{c^2k_\parallel^2}{\omega^2r_0^2}\left(\frac{1}{k_{T,1}^2}-\frac{1}{k_{T,2}^2}\right)^2, \quad (2)$$

where $J_m(k_{T,1}r)$ and $H_m^{(1)}(k_{T,2}r)$ represent mth-order Bessel and Hankel functions of the first kind, and

$$k_{T,i}=\sqrt{\left(\frac{\omega}{c}\right)^2\varepsilon_i-k_\parallel^2}, \quad i=1,2. \quad (3)$$

The prime on these functions denotes differentiation with respect to their argument. The speed of light in vacuum is denoted by c. The dispersion equation Eq. (2) differs qualitatively from that of a cylindrical PEC waveguide with radius r_0, for which we readily obtain $J_m'(k_{T,1}r_0)=0$ for transverse electric (TE) and $J_m(k_{T,1}r_0)=0$ for TM modes.[25] The propagating modes inside the cylindrical hole are calculated by solving for the roots of the dispersion equation, i.e., we numerically determine the $(\omega,k_\parallel)$ pairs that satisfy Eq. (2). The procedure involves a first coarse scanning of the $(\omega,k_\parallel)$ space to determine the approximate location of the dispersion relation. The solution is then refined to machine precision near the approximate location using Newton's method.[26]

In what follows, we assume that $\varepsilon_2(\omega)$ takes on the form of Eq. (1) with the collision frequency ω_τ set to zero. This amounts to a lossless plasmonic model. In addition, we set $\varepsilon_1=4$ (e.g., Si_3N_4) for a reason that will become apparent when we discuss the transmission calculations. Here, it suffices to point out that the cutoff for each mode in the dispersion diagram scales in inverse proportion to $\sqrt{\varepsilon_1}$, while the surface plasmon frequency varies in inverse proportion to $\sqrt{1+\varepsilon_1}$. Hence, from the results shown below one can easily infer the general behavior for any value of ε_1 for both the PEC and the plasmonic case.

For a hole radius $r_0=0.36\lambda_p$, where $\lambda_p=2\pi c/\omega_p$ is the plasma wavelength, the resulting dispersion relations are shown in Fig. 1. For the plasmonic model [Fig. 1(a)], we distinguish two types of modes: bulk modes, which extend into the metal region and lie above the line defined by $\omega^2=\omega_p^2+c^2k_\parallel^2$, and propagating waveguide modes, which are confined to the dielectric region of the waveguide. The latter exhibit two discrete bands labeled HE_{11} and EH_{11}, since we only consider modes with angular momentum $m=1$ so that they can couple to a normally incident plane wave. Unlike a PEC waveguide, the modes of a plasmonic waveguide are not purely TM or TE unless the angular momentum $m=0$. When $m\neq 0$, we designate the modes as HE_{mn} (EH_{mn}) when the H_z (E_z) component is dominant.

The fundamental HE_{11} mode lies completely below the surface plasmon frequency of the metal-dielectric interface. The vector plot of the electric field provides evidence that this mode has the correct symmetry to couple a normally incident plane wave. At $k_\parallel=0$, the cutoff frequency of the HE_{11} mode varies as a function of the hole radius. For the parameters used here, the normalized cutoff frequency is $\omega_c^{HE_{11}}=0.24\omega_p$ ($\lambda_c^{HE_{11}}=4.17\lambda_p$) for $\varepsilon_1=4$. When $k_\parallel\to\infty$, the frequency of the HE_{11} mode approaches the surface plasmon frequency $\omega_{sp}=\omega_p/\sqrt{\varepsilon_1+1}$.

The next-higher-order mode with $m=1$, which also couples to a normally incident plane wave (see vector plot of the electric field), is the EH_{11} mode. The band of this mode lies completely above the surface plasmon frequency. At $k_\parallel=0$, the cutoff frequency of the EH_{11} mode is $\omega_c^{EH_{11}}=0.63\omega_p$ ($\lambda_c^{EH_{11}}=1.59\lambda_p$) for $\varepsilon_1=4$. When $k_\parallel\to\infty$, the frequency of the EH_{11} mode approaches the light line in the dielectric. The dispersion diagram shows clearly that the HE_{11} and EH_{11} mode are separated by a stop band, which is located between the surface plasmon frequency and the EH_{11} mode cutoff frequency. Within the stop band, there are modes (TM_{01} and HE_{21}), but they do not couple to a normally incident plane wave.

Figure 1(b) shows the dispersion relations for the cylindrical PEC waveguide. For comparison purposes, we show only the fundamental TE_{11} mode and the TM_{11} mode. As can be inferred from the vector plots of their respective electric fields, these modes are the two lowest-order modes that couple to a normally incident plane wave. The TE_{11} mode cuts off at $\omega_c^{TE_{11}}=0.41\omega_p$ ($\lambda_c^{TE_{11}}=2.44\lambda_p$) for $k_\parallel=0$. Below this cutoff frequency, no propagating modes exist for a cylindrical PEC waveguide.[25] For $k_\parallel\to\infty$, the frequency behavior of the TE_{11} mode approaches that of the light line. Similarly, for the TM_{11} mode, the cutoff frequency at $k_\parallel=0$ is $\omega_c^{TM_{11}}=0.85\omega_p$ ($\lambda_c^{TM_{11}}=1.18\lambda_p$) and for $k_\parallel\to\infty$, the dispersion relation asymptotically approaches the light line.

The dispersion diagram of the plasmonic waveguide is quite distinct and qualitatively different from the PEC one. For example, the stop band between the two lowest-order propagating modes in the plasmonic waveguide is absent in the PEC model. The modes themselves also have distinct dispersion properties. The cutoff wavelength of the HE_{11} mode in the plasmonic waveguide is almost twice as long as the cutoff wavelength of the TE_{11} mode in the PEC waveguide. Hence, the plasmonic waveguide can sustain a propagating mode at a significantly longer cutoff wavelength than is to be expected from a PEC waveguide model. The qualitative difference in dispersion becomes particularly prominent for smaller holes. Figure 2(a) describes the evolution of the cutoff frequency (main panel) and wavelength (inset) for the fundamental mode as a function of hole radius for the PEC (dashed lines) and the plasmonic (solid lines) waveguide, respectively. For the PEC waveguide, the cutoff wavelength is proportional to the hole radius r_0 and remains so as the radius goes to zero. For the plasmonic waveguide, on the other hand, two different regimes of operation can be identified. In the "large"-hole regime, the behavior is quite similar to that of the PEC waveguide and differs only by a "fixed" offset in wavelength, which is approximately equal

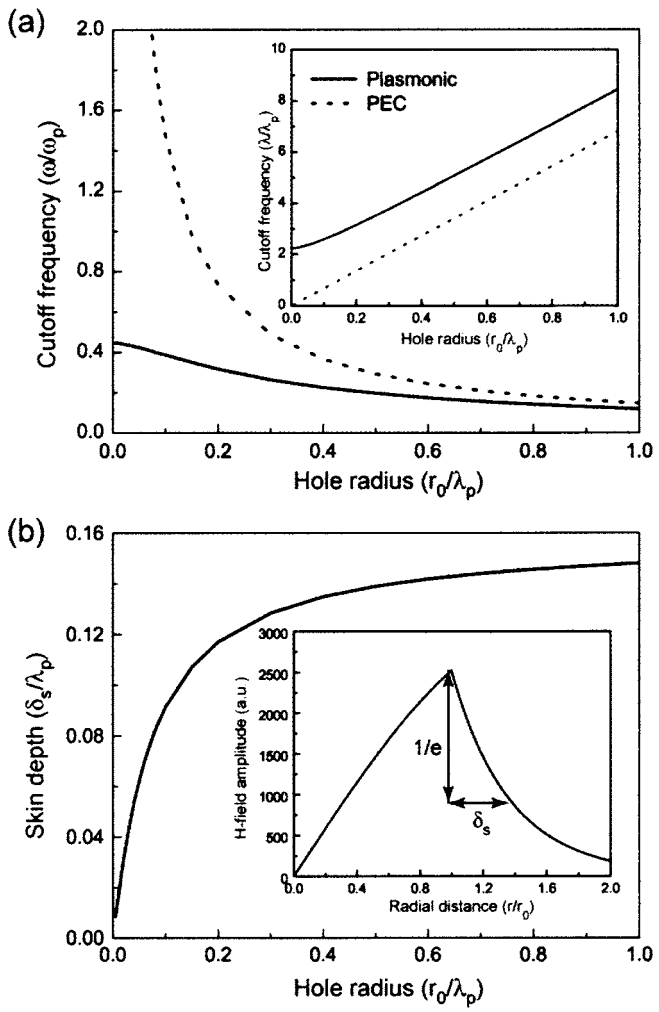

FIG. 2. (a) Cutoff frequency of the lowest-order waveguide mode versus hole radius r_0 for the PEC (TE_{11}, dashed line) and the plasmonic (HE_{11}, solid line) models, respectively. (b) Skin depth δ_s at the cutoff frequency for the plasmonic HE_{11} mode as a function of hole radius r_0.

to λ_p. In the "small"-hole region, however, the behavior of the plasmonic waveguide deviates significantly from the PEC result and the cutoff wavelength tends toward the surface plasmon wavelength inside the hole ($\sqrt{1+\varepsilon_1}\lambda_p$) when the hole radius goes to zero. This suggests that cylindrical holes in a plasmonic material can support propagating modes, regardless of how small the holes are. [Note that for holes that are sufficiently small, one needs to take into account the nonlocal nature or spatial dispersion of the complex dielectric function $\varepsilon_2(\omega,k)$, i.e., the plasmonic model is no longer valid.[27] However, for holes larger than 100 nm, we still expect the local dielectric function to be valid.[21]]

In addition to the difference regarding the presence or absence of a stop band, the cutoff behavior of the plasmonic waveguide cannot be explained by naively enlarging the PEC hole by a value proportional to the skin depth.[28] We have calculated the skin depth from the field profile of the HE_{11} mode at the cutoff for varying hole radius [see Fig. 2(b), inset]. Here, we define the skin depth δ_s as the distance inside the metal where the field magnitude drops to $1/e$ times its value at the dielectric-metal interface,

$$\frac{H_z(r=r_0+\delta_s)}{H_z(r=r_0)}=\frac{H_1^{(1)}[k_T(r_0+\delta_s)]}{H_1^{(1)}(k_T r_0)}=\frac{1}{e}. \tag{4}$$

Alternatively, one could define skin depth using the full magnetic field amplitude. Both definitions produce almost identical results. Figure 2(b) features the normalized skin depth δ_s/λ_p as a function of the normalized hole radius r_0/λ_p. For large hole radius, the skin depth is approximately constant and using it as an offset might be appropriate. For small hole radius, the skin depth decreases rapidly and vanishes as the hole radius goes to zero. This behavior is confirmed by an asymptotic analysis of Eq. (4): When $k_T r_0$ approaches zero, $H_1^{(1)}(k_T r_0)\to\infty$. In order for the left-hand side to be finite and nonzero, δ_s needs to go to zero as well. Hence, in the small-hole limit, the mode, in fact, does not penetrate into metal. In this regime, the plasmonic hole cannot be treated as a PEC hole with a larger effective radius. In contrast, our approach provides a consistent picture with small and large holes alike.

III. FDTD SIMULATION OF TRANSMISSION

Based upon the modal dispersion analysis above, we now consider the transport properties of a single hole and a hole array. In both cases, we assume a metal film with finite thickness h. We use a 3D total-field–scattered-field FDTD implementation in both simulations. For the single hole, uniaxial phase-matched layer (UPML) absorbing boundaries truncate the simulation domain in x, y, and z. For the hole array, UPML absorbing boundaries are applied in the z-direction and periodic Bloch boundaries in x and y. For the single-hole simulation, we apply a normally incident pulsed Gaussian-beam excitation centered at 500 nm to obtain the response in the ultraviolet and visible wavelength range within a single simulation. The Gaussian beam has a transverse spatial full width at half maximum of 1 μm. The incidence plane is chosen a few 100 nm above the metallic film and the field data for determining the spectral transport properties of the waveguide, through direct integration of the Poynting vector, are collected in an observation plane placed in the middle of the metallic film. Such a calculation measures the total amount of power that can pass through the hole. The transmittance is defined as the ratio of the power through the waveguide in the metallic film to the incident power.

Figure 3 shows the spectral transmittance of a cylindrical hole ($r_0=50$ nm$=0.36\lambda_p$) in a 250-nm-thick metal film, modeled as a PEC (dashed blue line) and a plasmonic material (solid red line), respectively. For the plasmonic material, we assume a plasma wavelength $\lambda_p=138$ nm ($\omega_p=1.37\times10^{16}$ rad/s) and a collision frequency $\omega_\tau=7.29\times10^{13}$ rad/s.[29] The presence of a nonzero collision frequency leads to losses and we can calculate the decay length $L_d=1/2k_\parallel''$, using the complex wave number of the mode, $k_\parallel=k_\parallel'+ik_\parallel''$. The decay length is approximately 2–3 μm for most of the wavelength range covered by the HE_{11} mode. Hence, the HE_{11} mode can propagate over a distance that is relevant for transport through metallic films that are a few

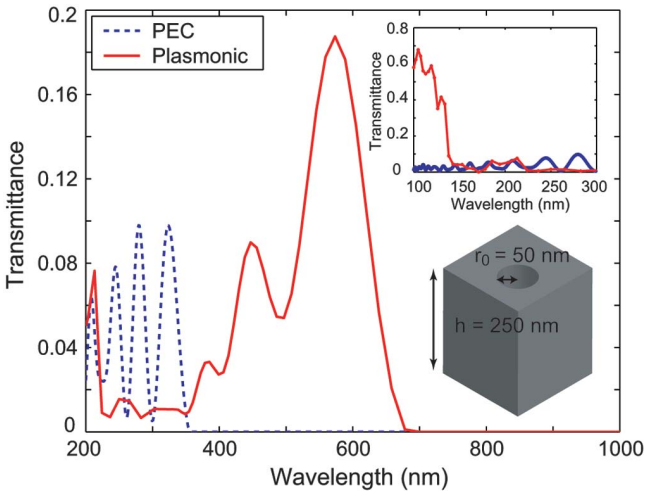

FIG. 3. (Color) The solid red line corresponds to the transmission spectrum of a single cylindrical hole (r_0=50 nm=0.36λ_p) in a 250-nm-thick metal film as shown in the inset. The metal is modeled as a plasmonic material with λ_p=138 nm (ω_p=1.37 $\times 10^{16}$ rad/s) and ω_τ=7.29$\times 10^{13}$ rad/s. The hole is filled with a dielectric (ε_1=4). The dashed blue line is the transmission spectrum for the same geometry, except that the metal is modeled as a PEC. The inset shows the detailed transmission spectrum from λ=100 to 300 nm.

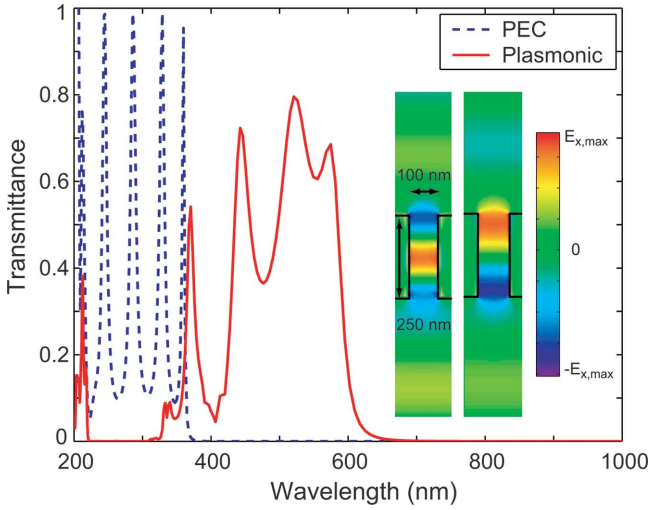

FIG. 4. (Color) The solid red line corresponds to the transmission spectrum T of a 50-nm-radius cylindrical hole array with 180 nm period (in x and y) in a 250-nm-thick metal film. The metal film and the dielectrics are modeled in accordance with the single-hole case of Fig. 3. Insets show E_x field profile along the hole for the two major peaks at wavelengths 442 nm (T=0.72, left panel) and 520 nm (T=0.79, right panel), respectively, with light incident from the top. (The simulation domain used in the 3D FDTD calculation measures 180$\times$180$\times$1000 nm^3.) The field pattern clearly shows the existence of propagating modes. The dashed blue line is the transmission spectrum for the same geometry, except the metal is modeled as a PEC.

hundreds of nanometers thick. (We note that the same conclusion holds when we repeat the calculation using tabulated data for the dielectric function of silver.[30]) We fill the holes with a dielectric (ε_1=4) while the film is surrounded by vacuum. In the PEC case, the spectral transmittance is approximately constant and then falls off at the cutoff wavelength $\lambda_c^{TE_{11}} \cong 3.41\sqrt{\varepsilon_1} r_0$=341 nm, which is determined by the radius of the hole and the dielectric constant of the material inside the hole. In the plasmonic case, using the Drude free-electron model in Eq. (1) including losses, the transmittance depends on a combination of hole geometry and dielectric and metal properties. It features a region of high transmission (Fig. 3, inset) below the bulk plasma wavelength (λ_p=138 nm). It is well known that in this region the bulk metal behaves as a dielectric and becomes transparent. Due to the EH_{11} mode, the transparency region continues until λ=220 nm, in agreement with the dispersion diagram. Adjacent to this high-transmission region is a region of zero transmission, which ranges from 220 to 350 nm. Past the stop band there is a passband with a cutoff at $\lambda_c^{HE_{11}}$ =600 nm. This passband is due to the fundamental HE_{11} mode. Both the stop band and the passband beyond it are unique transmission features resulting from the plasmonic dispersion diagram. In fact, the onset and cutoff of each of these features compare well with the values obtained from the dispersion calculation. In comparison with the PEC case, the HE_{11} passband lies entirely beyond the PEC cutoff. The peak amplitude of the transmittance is larger than the peak amplitude in the PEC case. Its cutoff wavelength $\lambda_c^{HE_{11}}$ is almost twice as large as $\lambda_c^{TE_{11}}$ and features a decaying tail. We also emphasize the absence of a stop band in the PEC-based transmission spectrum. Simulations without loss component in the plasmonic model revealed that the transmission spectrum is quasi-independent of material losses (mean difference $<$10%). This is consistent with long decay lengths, which are on the order of micrometers for the plasmonic model, compared to the 250 nm thickness of the film. The importance of propagating modes in the transmission properties of subwavelength cylindrical holes is also evident for appropriately designed hole array structures. Previously, transmission enhancement for such structures has been largely associated with the resonant excitation of surface waves and evanescent tunneling through the holes.[9,11,13–16] Here, instead, we explore a different regime in which the propagating waveguide mode provides the dominant transport mechanism. For simplicity, we consider only plane waves incident along the normal direction. The signature of a propagating waveguide mode in the transmission will be most noticeable when the HE_{11} band covers a wavelength range where no other competing mechanisms are present. Hence, the wavelengths of a surface wave resonance at normal incidence, due to the folding of the dispersion curve of the top and bottom surfaces,[9] should be below the smallest wavelength of the HE_{11} band, which corresponds to the surface plasmon wavelength inside the hole. For this to occur, the array needs to have a periodicity that is substantially smaller than what has been featured in recent experiments. Figure 4 shows the transmittance spectrum T for an array of cylindrical holes, which has been designed according to aforementioned principles. It features an array of 50-nm-radius cylindrical holes in a 250-nm-thick metal film. The periodicity of the array is 180 nm and the holes are filled with a dielectric (ε_1=4), while the film is surrounded by

vacuum. For the PEC model, this array has a transmission spectrum with a cutoff wavelength of 370 nm, which is close to the cutoff wavelength for a single dielectric-filled hole. Below that wavelength, the transmission band features a series of high-finesse Fabry-Pérot resonances. In contrast, the spectrum of the plasmonic model (with the same parameters as in the single-hole case) shows a clear passband ranging from 350 to 600 nm that lies entirely beyond the PEC cutoff wavelength. This range, as well as the stop band between 220 and 320 nm, once more agrees well with the dispersion relation of a single hole. The insets show the E_x field profile along the aperture for the peaks at wavelengths 442 nm ($T=0.72$, left panel) and 520 nm ($T=0.79$, right panel). The field pattern clearly demonstrates the existence of propagating modes. Also, the transverse field profile inside the hole obtained from the FDTD method agrees well with the one obtained from the dispersion calculation in Fig. 1.

IV. CONCLUSION AND DISCUSSION

To the best of our knowledge, this work shows for the first time the importance of a plasmonic-based dispersion relation for the transport of incident light through subwavelength cylindrical holes in a metallic film. We find that the dispersion diagram exhibits three distinct features that have a profound impact on the transmission of incident light through cylindrical holes. First, such holes always support propagating modes near the surface plasmon frequency, regardless of how small the holes are. Second, the fundamental HE_{11} mode, which couples to an external normally incident plane wave, is located completely below the surface plasmon frequency of the metal. Thus, a cylindrical hole in a plasmonic metal always exhibits a passband below the surface plasmon frequency. Third, when the radius of the hole is small, there exists a stop band, just above the surface plasmon frequency, where light does not transmit. Hence, a single hole may behave as a bandpass filter and allow longer wavelengths to pass through while rejecting shorter ones. All of these features are fundamentally different from the dispersion behavior assuming a PEC model and lead to qualitatively different transmission properties. Our results show the potential of using propagating modes to obtain high transmission with subwavelength holes. In Fig. 4, the plasmonic passband features a peak transmission of 0.79, which is approximately an order of magnitude higher when compared with previously published transmission in hole arrays. The use of small periodicity (approximately 200 nm) means that for all wavelengths of practical interest the array is diffraction-free while allowing for a bigger packing density of holes and potentially a smaller footprint. These benefits are likely to be important for practical applications.

ACKNOWLEDGMENTS

This work was supported in part by National Science Foundation Grant No. ECS-0134607 and by AFOSR Grant No. FA9550-04-1-0437. H.S. acknowledges the support of Samsung Lee Kun Hee Foundation.

[1] For the latest developments, see, for example, Opt. Express **12**, 3618 (2004), focus issue.
[2] J. A. Porto, F. J. Garcia-Vidal, and J. B. Pendry, Phys. Rev. Lett. **83**, 2845 (1999).
[3] F. I. Baida and D. Van Labeke, Phys. Rev. B **67**, 155314 (2003).
[4] Y. Takakura, Phys. Rev. Lett. **86**, 5601 (2001).
[5] E. Popov, M. Neviere, S. Enoch, and R. Reinisch, Phys. Rev. B **62**, 16100 (2000).
[6] S. Astilean, P. Lalanne, and M. Palamaru, Opt. Commun. **175**, 265 (2000).
[7] P. Lalanne, J. P. Hogonin, S. Astilean, M. Palamaru, and K. D. Moller, J. Opt. A, Pure Appl. Opt. **2**, 48 (2000).
[8] Q. Cao and P. Lalanne, Phys. Rev. Lett. **88**, 057403 (2002).
[9] T. W. Ebbesen, H. J. Lezec, H. F. Ghaemi, T. Thio, and P. A. Wolff, Nature (London) **391**, 667 (1998).
[10] D. E. Grupp, H. J. Lezec, T. W. Ebbesen, K. M. Pellerin, and T. Thio, Appl. Phys. Lett. **77**, 1569 (2000).
[11] L. Martin-Moreno, F. J. Garcia-Vidal, H. J. Lezec, K. M. Pellerin, T. Thio, J. B. Pendry, and T. W. Ebbesen, Phys. Rev. Lett. **86**, 1114 (2001).
[12] W. L. Barnes, W. A. Murray, J. Dintinger, E. Devaux, and T. W. Ebbesen, Phys. Rev. Lett. **92**, 107401 (2004).
[13] W. L. Barnes, A. Dereux, and T. W. Ebbesen, Nature (London) **424**, 824 (2003).
[14] A. Krishnan, T. Thio, T. J. Kima, H. J. Lezec, T. W. Ebbesen, P. A. Wolff, J. Pendry, L. Martin-Moreno, and F. J. Garcia-Vidal, Opt. Commun. **200**, 1 (2001).
[15] J. B. Pendry, L. Martin-Moreno, and F. J. Garcia-Vidal, Science **305**, 847 (2004).
[16] H. J. Lezec and T. Thio, Opt. Express **12**, 3629 (2004).
[17] C. F. Bohren and D. R. Huffman, *Absorption and Scattering of Light by Small Particles* (Wiley, New York, 1983).
[18] M. A. Ordal, R. J. Bell, R. W. Alexander, Jr., L. L. Long, and M. R. Querry, Appl. Opt. **24**, 4493 (1985).
[19] M. A. Ordal, L. L. Long, R. J. Bell, S. E. Bell, R. R. Bell, R. W. Alexander, Jr., and C. A. Ward, Appl. Opt. **22**, 1099 (1983).
[20] A. D. Rakic, A. B. Djurisic, J. M. Elazar, and M. L. Majewski, Appl. Opt. **37**, 5271 (1998).
[21] L. Novotny and C. Hafner, Phys. Rev. E **50**, 4094 (1994).
[22] F. de Abajo, Opt. Express **10**, 1475 (2002).
[23] F. J. Garcia-Vidal and L. Martin-Moreno, Phys. Rev. B **66**, 155412 (2002).
[24] C. A. Pfeiffer, E. N. Economou, and K. L. Ngai, Phys. Rev. B **10**, 3038 (1974).
[25] D. M. Pozar, *Microwave Engineering* (John Wiley & Sons, New York, 1997).
[26] Computer code MATHEMATICA (Wolfram Research, Inc., Champaign, IL, 2004).
[27] G. C. Aers, A. D. Boardman, and B. V. Paranjape, J. Phys. F: Met. Phys. **10**, 53 (1980).
[28] L. Martin-Moreno and F. J. Garcia-Vidal, Opt. Express **12**, 3619 (2004).

[29] This represents a commonly used model for silver and is approximately valid in the near-infrared region with wavelengths down to 500 nm. In addition, we choose $\varepsilon_1=4$ such that at least the lower cutoff wavelength is still within the region of validity. In any case, the goal here is to investigate the general behavior of the plasmonic material model. The subtleties of the interband transitions, specific to noble metals, will be addressed in later work.

[30] E. D. Palik and G. Ghosh, *Handbook of Optical Constants of Solids* (Academic Press, Orlando, FL, 1985).